DOI: 10.1002/ejoc.200701053

Synthesis, Optical Properties and Magnetic Studies of 2,6-Bis(pyrazolylmethyl)-pyridine Functionalized with Two Nitronyl Nitroxide Radicals

Giorgio Zoppellaro,[a,b] Ahmed Geies,[a] K. Kristoffer Andersson,[b] Volker Enkelmann,[a] and Martin Baumgarten*[a]

Keywords: High-spin molecules / Radicals / EPR spectroscopy / Bis(pyrazolylmethyl)pyridine / NMR spectroscopy

The synthesis, optical properties, spin-polarization path and magnetic ground-state studies of a novel nitronyl nitroxide biradical system based on the 2,6-bis(pyrazolylmethyl)pyridine unit is reported. Besides the presence of σ conjugation and a non-alternant pathway for spin polarization through the core as a coupling unit, the through-bond ferromagnetic interaction between spin carriers, although weak ($0.06\ cm^{-1} < \Delta E_{ST} = 2J/k_B < 0.6\ cm^{-1}$), is preserved. It vanishes ($2J/k_B \approx 0$) upon coordination with Zn^{2+} metal ions, but is restored upon Zn^{2+} depletion with EDTA.

Introduction

Nitronyl (NN) and iminonitroxide (IN) free radicals were described in the 1970s by Osiecki and Ullman and their coworkers in their pioneering work[1–3] and since then they have attracted increasing attention with a revival in the 1990s. The increase in interest mainly stems from the use of these stable radical units as building blocks in the design of molecular magnetic materials,[4] such as purely organic ferromagnetically ordered solids,[5] metal–organic exchange-coupled complexes,[6] as well as new agents for biomedical applications (e.g., in bioimaging and selective NO scavengers).[7] The synthesis of these radical synthons relies on the condensation of 2,3-bis(hydroxyamino)-2,3-dimethylbutane[8] with carbaldehyde residues followed by the oxidation of the condensation products. The challenge in this field[9] consists of assembling functional derivatives such that interactions between spin carriers can be controlled and tailored at will through the rational design of the molecular backbone (CU).[10] Theories based on topological principles allowed prediction of the magnetic ground state in non-Kekulé hydrocarbons[11] and have guided the synthetic design so far. However, these principles have their limitations[12] as they are not readily extended to non-alternant systems and heteroatom-containing radicals or couplers. Previously we demonstrated that functionalization of the 4′,4′′-positions of the bispyrazolylpyridine core **A** (Figure 1) with neutral NN radical moieties[13] gated intramolecular ferromagnetic exchange interaction ($\Delta E_{ST} = 11.8 \pm 4.8\ cm^{-1}$), besides the unfavourable exchange coupling path and the distance between the radical units (ONĈNO groups ca. 8.3 Å). This represented the first reported example of coupled ($S = 1$) Ullman radicals connected to a 2,6-bispyrazolylpyridine unit.[14] In order to gain knowledge of the dominant spin-polarization pathway in similar hetero systems, we decreased the π conjugation in **A** by adding two C(sp^3) bonds between the pyrazolyl moieties and the central pyridine ring. The design led to **B** {2,6-bis[4-(1-oxyl-3-oxido-4,4,5,5-tetramethylimidazolin-2-yl)pyrazolylmethyl]pyridine}, a σ-conjugated biradical system. Whereas biradical **A** embraces a rigid scaffold, **B** can adopt several molecular conformations, especially in solution, but such conformational freedom can also be constrained after coordination of a metal ion to the pyridyl-pyrazolyl nitrogen donors. Despite the presence of two saturated carbon centres (sp^3) and a non-alternant path for the spin polarization, through-bond fer-

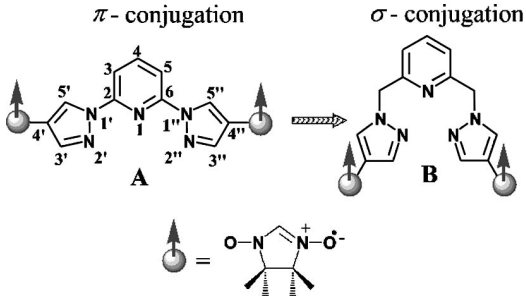

Figure 1. Switching from π (**A**) to σ conjugation (**B**) in nitronyl nitroxide (**NN**) biradical systems connected to heterocyclic coupling units.

[a] Max Planck Institute for Polymer Research,
Ackermannweg 10, 55128 Mainz, Germany
Fax: +49-6131-379370
E-mail: baumgart@mpip-mainz.mpg.de
[b] Department of Molecular Biosciences, University of Oslo,
Box 1041, Blindern, Norway
Supporting information for this article is available on the WWW under http://www.eurjoc.org/ or from the author.

romagnetic interaction between spin carriers is still preserved ($0.06\ cm^{-1} < \Delta E_{ST} = 2J/k_B < 0.6\ cm^{-1}$). This exchange coupling is then lost ($2J/k_B \approx 0$) upon coordination with the Zn^{2+} metal ion, rendering such a weakly coupled spin system a promising spin-probe for metal recognition in solution with potential biological applications.

Results and Discussion

Synthesis and Optical Properties of B

The assembly of diradical **B** is illustrated in Scheme 1 and started with the synthesis of the dicarbaldehyde precursor **3** which was obtained by a multistep approach that involved a coupling reaction between 4-formyl-1*H*-pyrazole (**1**) and 2,6-bis(bromomethyl)pyridine (**2**) in the presence of NaH using THF as the reaction solvent. The detailed synthesis of **1** has been reported previously.[13,15] The nucleophilic substitution occurred very quickly (3 h) and provided 2,6-bis[(4-formylpyrazolyl)methyl]pyridine (**3**) in a fair yield (54%) after recrystallization from EtOH/H_2O solution.

The condensation of **3** with 2,3-bis(hydroxyamino)-2,3-dimethylbutane (**4**) was carried out in $CHCl_3$/MeOH and gave 2,6-bis[4-(1,3-dihydroxy-4,4,5,5-tetramethylimidazolidin-2-yl)pyrazolylmethyl]pyridine (**5**) as a white precipitate in two days (yield 62%). The diamagnetic precursor **5** was oxidized to the biradical **B** by sodium periodate under phase-transfer conditions ($CHCl_3/H_2O$). Side-products were easily recognized by TLC, and **B** was finally purified by flash chromatography (acetone/petroleum ether, R_f = 0.28) on a SiO_2 column (yield 64%).

Biradical **B** is exceptionally stable as a solid and in aprotic solutions in which it can be stored for a year without decomposition. The UV/Vis spectrum of **B** is shown in Figure 2 together with those of the bis(pyrazolyl)pyridine NN biradical **A** and the pyrazol-4-yl nitronyl nitroxide monoradical,[16] **PzNN**, used as a reference. **B** exhibits an intense band in the visible absorption region characterized by several vibronic components (toluene, λ_{max} = 651 nm, ε = 2420 $M^{-1}cm^{-1}$, n→π*) with an intensity roughly twice that shown by the monoradical **PzNN** (toluene, λ_{max} = 647 nm, ε = 1120 $M^{-1}cm^{-1}$, n→π*). The π→π* transition of the aminoxyl oxide group appears at λ_{max} = 352 nm (ε = 44060 $M^{-1}cm^{-1}$), considerably blue-shifted with respect to the same transition observed in the bis(pyrazolyl)pyridine biradical **A** in which the methylene bridge is absent (λ_{max} = 375 nm, ε = 16960 $M^{-1}cm^{-1}$). This finding emphasizes the effect of the σ-CH_2 bonds on hampering π conjugation between radical units through the coupling unit core. As the spin-polarization mechanism is effected by the π electrons

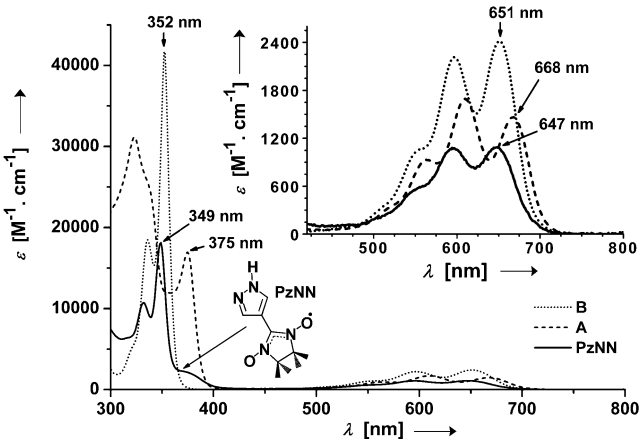

Figure 2. UV/Vis absorption spectra recorded in toluene solutions for **B**, **A** and **PzNN**.

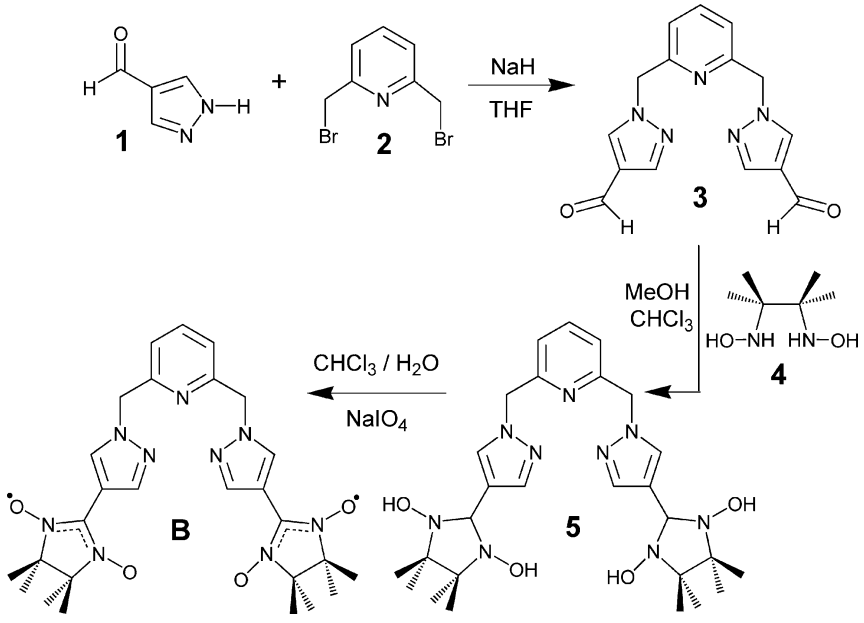

Scheme 1. Synthetic approach to biradical **B**.

in the doubly filled MOs, destabilization of the triplet in **B** relative to **A** is anticipated. The π→π* transition observed in **B** is on the other hand slightly red-shifted compared with the same transition characterizing the monoradical **PzNN** (λ_{max} = 349 nm, ε = 18100 $M^{-1}cm^{-1}$) and indicates that a small conjugation between spin carriers is still present. The other characteristic spectroscopic fingerprint of the radical centres appears in the infrared absorption spectrum, as shown in Figure 3. After oxidation of the radical precursor **5**, the intense and broad absorption at around 3200 cm^{-1} originating from the –NH–OH residues (ν_{NH-OH}) disappears in **B** and the so-formed aminoxyl oxide moieties show a distinctive strong ν_{N-O} stretching vibration at 1365 cm^{-1}, which is consistent with literature values, both in frequency and intensity.[13,17,18]

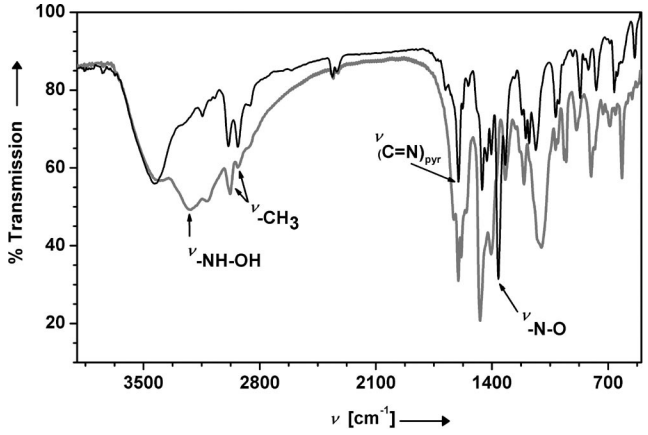

Figure 3. FTIR spectra (KBr pellet) of the radical precursor **5** (grey line) and the biradical **B** (black line) recorded at T = 293 K.

Paramagnetic ^{1}H NMR Analysis of B

The solution paramagnetic ^{1}H NMR spectrum of a liquid solution of **B** is shown in Figure 4. It provides experimental information about the sign (positive or negative) of the spin densities (ρ) on the carbon centres, especially those adjacent to the protons experiencing paramagnetic shifts.[19] By comparison with the hydrogen resonances observed for the diamagnetic precursor **5**, it was found that the pyrazole –CH hydrogen atoms exhibit a broad and very weak downfield signal at about +36 ppm. These hydrogen atoms have positive couplings ($+a_H$), which indicates negative spin densities (ρ^-_C) on the C2 carbon atoms. The methylene ($–CH_2–$, –0.9 ppm) and the imidazolylmethyl protons ($–CH_3$, –16 ppm) also exhibit broad signals but their intensities are very strong and upfield shifted ($–a_H$), thus positive spin densities (ρ^+_C) are located on C1 and C3. Noteworthy, the pyridyl protons at C4 and C5 overall feature very small paramagnetic shifts ($|\Delta\delta| \leq 0.3$ ppm) compared with their resonances in **5** and are accompanied by signal broadening (ca. 300 Hz). These observations highlight the effect induced by C(sp^3) bonds, strongly hindering but not entirely disrupting spin-polarization transfer from the radical units to the pyridyl spacer.

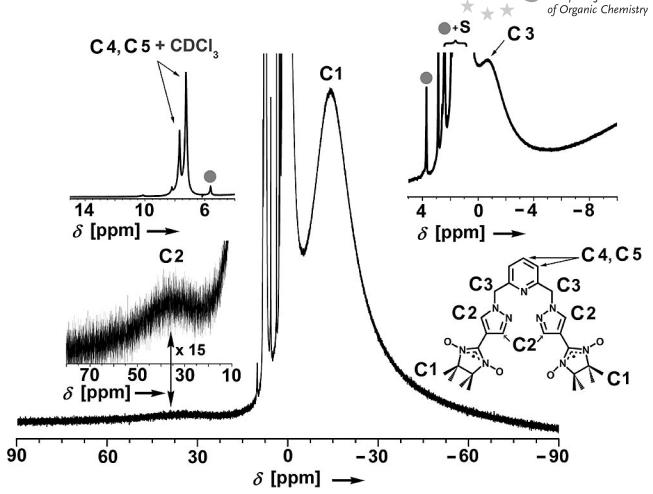

Figure 4. The paramagnetic ^{1}H NMR (300 MHz, T = 293 K) spectrum of **B** (2×10^{-2} M) recorded in $CDCl_3$. The signals marked with ● and **S** in the insets correspond, respectively, to diamagnetic impurities and residual solvent peaks.

Crystal Structure of B

Upon slow diffusion of hexane into a $CHCl_3$ solution of radical **B**, a blue crystalline material formed within three days which was characterized by X-ray diffraction. Two molecules are present in the asymmetric unit, labelled as [1] and [2] in Figure 5, and 12 molecules form the crystallographic unit cell. The structural data and solution refinements are summarized in Table 1. The torsional angles between the imidazolidinylpyrazolyl rings in [1] and [2] reflect the possibility of free rotation around one of the single bonds and hence can be used as a measure of the effective π conjugation through the spacer. In unit [1] the N15–C38–C36–C35 angle is 0.74°, whereas in [2] the N4–C10–C8–C9 angle is –0.24° and N8–C21–C19–C18 is 0.0°. Therefore [1] and [2] exhibit imidazolidinyl and pyrazolyl rings that are nearly coplanar, which in turn should induce very efficient spin-polarization transfer from the radicals into the pyrazolyl moieties. The intra-ring torsion angles of the imidazolidinyl rings are 10.3° for [1] and between –5.9 and –10.0° for [2]. The N–O bond lengths are consistent with literature values reported for nitroxide radicals (1.275–1.290 Å). The introduction of two C(sp^3) bonds ($–CH_2–$ carbon atoms) induces the formation of a step-like packing structure, as shown in Figure 6. A similar conformation, described as Z-like by the authors, has been found recently in another biradical system in which a butyl group was used as the spacer for two pyazolyl-NN radical moieties.[20] In unit [1] the N13–N12–C34–C31 angle reaches 67.2°, whereas in [2] the N7–N6–C17–C5 angle is –62.9° and N3–N2–C6–C1 –67.1°. Such torsion angles should lead to a break down in spin-polarization transfer through the pyridine ring, hence hindering even more the through-bond interaction between the two ancillary S = ½ spins. The intramolecular distance between the ONĈNO groups (C38–C*38) in [1] is 11.624 Å and that between the 4′,4′′-pyrazolyl carbon atoms (C36–C*36) is 9.695 Å. In [2] the intramolecular distance between ONĈNO groups (C21–C10) is larger, 11.842 Å, as is the

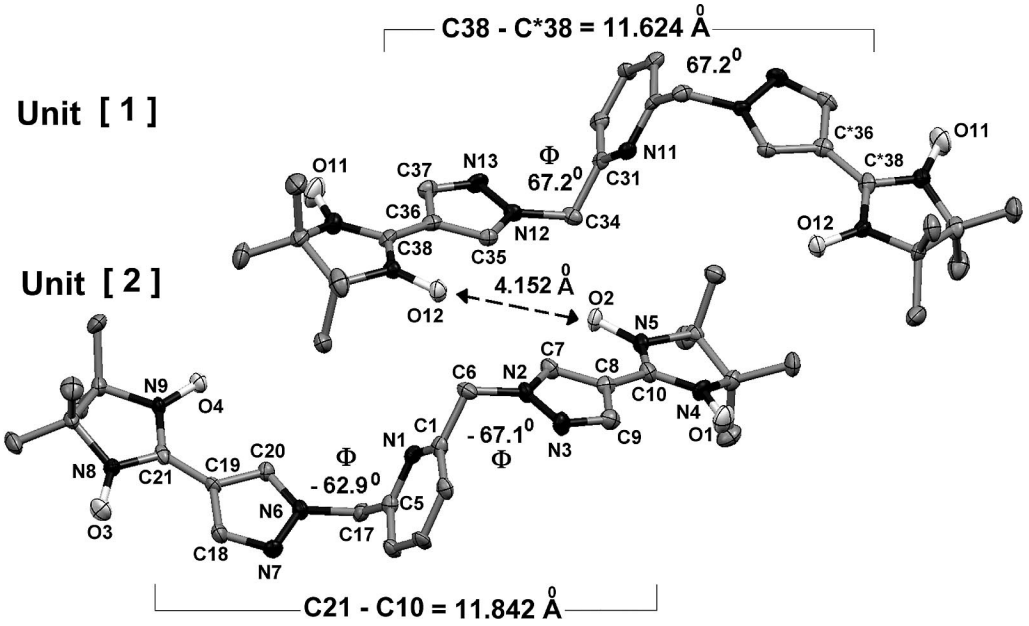

Figure 5. Crystal structure of **B** showing the dimeric form with units [1] and [2]. The thermal ellipsoids are drawn at the 50% probability level. The hydrogen atoms have been omitted for clarity. Relevant –NO···ON– distance and dihedral angles are also depicted.

distance between the 4′,4′′-pyrazolyl carbon atoms (C19–C8), 9.841 Å. In the [1]–[2] asymmetric unit, as depicted in Figure 5, the shortest intermolecular through-space distance between the imidazolidinyl oxygen atoms is 4.152 Å. Although such a distance is greater than a standard van der Waals contact, it is still close enough to promote a non-negligible antiferromagnetic interaction between [1] and [2]. This is due to the fact that the N–O groups carry the largest size and same spin-density sign. Several short magnetic contacts (<3 Å) are present in the asymmetric unit and are depicted by broken lines in Figure 7. The signs determined for the spin densities experimentally by ^{1}H NMR paramagnetic shift analysis allow the nature of such through-space couplings to be defined (ferro, ***F***, or antiferromagnetic, ***AF***), the labels + and – in Figure 7 indicating positive and negative spin densities located on the individual atoms. In total, five ***AF*** (spin densities of the same sign, +···+ or –···–) and four ***F*** interactions (opposite signs, +···–) are relevant here to describe the magnetic properties of the bulk material. However, it is worth noting that the magnitude of the interaction $|J/k|$ depends on both the distance and the orientation between the atoms with non-zero spin density (ρ) and also on the product ($\rho_A\rho_B$) at the interacting atoms. The ***AF*** interactions O2···H351 (2.585 Å) and O12···H71 (2.620 Å)

Table 1. X-ray data for **B**, experimental details, structure solutions and refinements.

Formula	$C_{27}H_{35}N_9O_4$
M	549.63
Crystal system	monoclinic
Space group	C_2/c (no. 15)
a [Å]	26.3720(8)
b [Å]	13.5650(6)
c [Å]	23.5650(8)
α [°]	90
β [°]	100.0630(13)
γ [°]	90
V [Å^3]	8300.4(5)
Z	12
Abs. coeff. [mm^{-1}]	0.092
$\rho_{calcd.}$ [g cm^{-3}]	1.319
$F(000)$	3504.0
Crystal size [mm]	$0.08 \times 0.24 \times 0.41$
Colour	blue
Shape	prism
Temperature [K]	293
Radiation, λ [Å]	Mo-K_α, 0.71073
Θ range [°]	4.091–29.499
h,k,l max.	36,18,32
$N_{refl.}$	8854
R (reflections)	0.0720(5936)
wR_2 (reflections)	0.0781(5936)
$N_{par.}$	544
R_1[a]	0.0405
wR_2[b]	0.0448
GOF	0.856

[a] $R_1 = \Sigma||F_o| - |F_c||/\Sigma|F_o|$. [b] $wR_2 = \{\Sigma w(|F_o| - |F_c|)^2/\Sigma w|F_o|^2\}1/2$.

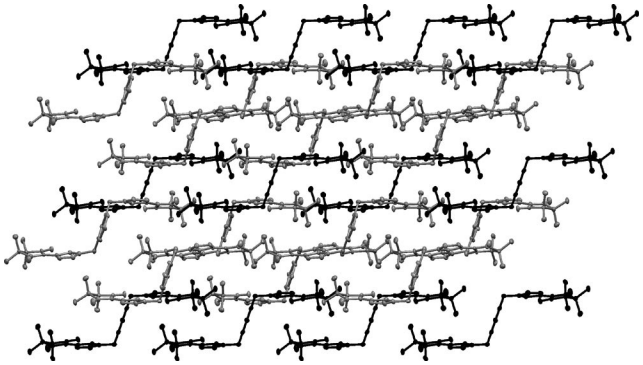

Figure 6. Molecular packing of **B** viewed down the crystallographic b axis. Unit [1] is depicted in black and [2] in light grey.

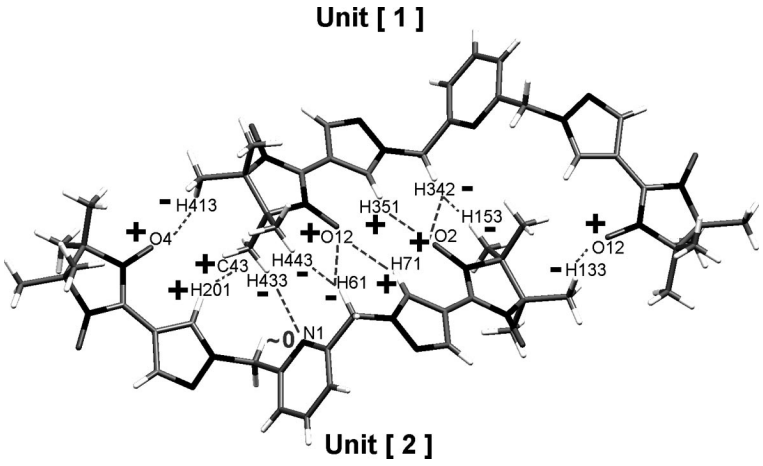

Figure 7. Sketch of the through-space interactions (magnetic contacts) between units [1] and [2] in **B**.

are expected to be much stronger than those present between O12···H61 (2.465 Å) (***F***) and O2···H342 (2.444 Å) (***F***). The other contacts H342···H153 (2.384 Å), H61···H443 (2.394 Å) and H201···C43 (2.900 Å), all ***AF***, should be relatively weak or at least weaker than the ***F*** contacts O4···H413 (2.644 Å) and O12···H133 (2.623 Å) because the products $\rho_A\rho_B$ are larger in the latter cases. It is anticipated that the magnetic properties of the bulk material should be governed by the ***AF*** terms. This is shown by the bulk susceptibility measurements carried out on the crystalline material of **B** reported below.

EPR and Bulk Susceptibility Analyses of B

The solution EPR spectrum of **B** (see A in Figure 8, toluene, 10^{-4} M, solid line) exhibits a rather clear nine-line

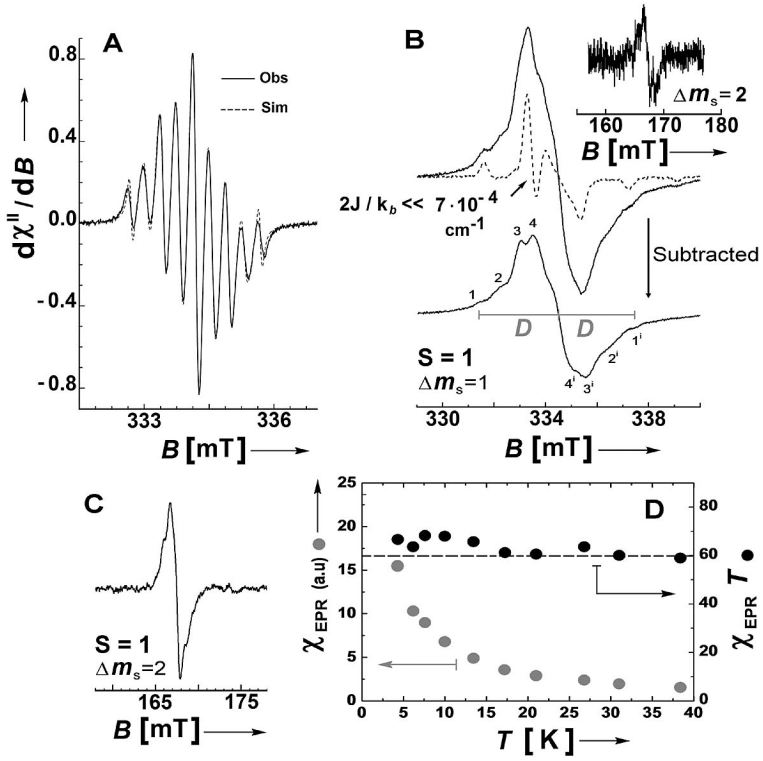

Figure 8. (A) X-band EPR spectrum of **B** recorded in toluene solution at T = 293 K (solid line) and its simulation (dotted line). (B) EPR spectrum of **B** in the frozen state recorded at T = 122 K (upper solid line). The dotted spectrum shows the EPR envelope arising from the out-of-phase component $|J/a_N| << 1$ while the lower spectrum (subtracted) represents the biradical envelope under a strong exchange limit ($|J/a_N| \geq 40$). The inset shows the Δm_s = 2 transition recorded at T = 122 K. (C) The Δm_s = 2 transition recorded at T = 4.1 K. (D) χ_{EPR} (●) and $\chi_{EPR}T$ (●) vs. T for the double-integrated Δm_s = 2 transition recorded in the low-temperature range (T < 40 K.) The dashed line is a guide to the eyes for ΔE_{ST} = 0.

pattern with g_{iso} = 2.0065(1) and reveals a through-bond exchange interaction between the radical units with $|J/a_N| >> 1$.[21] Although the spectral width and peak positions did not show solvent dependency, apart from a decreased solubility of **B** in less polar environments (e.g., hexane), an alternating line-width effect became visible upon sample cooling from 272 to 211 K; this is due to the occurrence of different rotamers in solution which modulate the time-dependent exchange term $J(t)$ around its time-averaged $<J>$.[22] The simulation of the solution EPR spectrum recorded at room temperature (part A in Figure 8, dotted line) was obtained by numerical diagonalization of the spin-Hamiltonian $\hat{H}$ [Equation (1)] and provides an estimate of the lower limiting value for the exchange energy J, but not its sign ($|J|$).

$$\hat{H} = g\beta_e B_o \hat{S}_{a,b} - 2J\hat{S}_a\hat{S}_b + \sum_{ij} a_N ij(\hat{S}_a\hat{I}_{N_{ij}} + \hat{S}_b\hat{I}_{N_{ij}}) \quad (1)$$

The simulation result accounts for a percentage (25%) of the uncoupled biradical ($|J/a_N| << 1$), resulting from out-of-phase modulation effects, superimposed on the biradical component (75%) under a strong exchange limit with $|J/a_N| \geq 40$ (i.e., $|2J/k_B| \geq 0.056\ cm^{-1}$), a nitrogen hyperfine splitting a_N of 20.94 MHz and a Gaussian line-width (l_w) of 6.00 MHz. In frozen solution (T = 122 K, 10^{-3} M in toluene) a poorly resolved zero-field-splitting (zfs) signal (Δm_s = 1) characterizes **B** (g_{av} = 2.007), as shown in Figure 8 (B), but the forbidden half-field Δm_s = 2 transition (g_{av} = 4.01, $m_s = -1 \rightarrow m_s = +1$) was detected demonstrating its triplet-state (S = 1) nature (B in Figure 8, upper inset). The double-integrated Δm_s = 1 signal, recorded under non-saturating conditions, accounts for 2.0 ± 0.1 uncorrelated spins. Thus a small energy difference between singlet and triplet states characterizes **B** and at T = 122 K its spin population still follows the Boltzmann distribution.

In order to obtain further information on the zfs magnitude $|D/hc|$ of the biradical fraction under a strong exchange limit, we performed on **B** variable power saturation experiments (T = 122 K, b = 0.47 ± 0.01, $P½$ = 0.82 ± 0.06 mW, R^2 = 0.999) and the results were compared with the saturation behaviour of the **PzNN** monoradical (T = 122 K, b = 1.05 ± 0.01, $P½$ = 0.71 ± 0.04 mW, R^2 = 0.999). The observed trends were analysed according to the theory of Portis and Castner (see the Exp. Sect.), where b represents the relaxation factor and $P½$ the power at which half of the signal is saturated.[23] The magnetic behaviours and the resulting fittings are plotted in Figure 9. It should be noted that in the case of both exchange-coupled systems and in the presence of dipolar interactions, the relaxation factor b is usually found to be less than 1, as observed here for **B**.[24,25] From the microwave saturation results it is assumed that the uncoupled biradical component in **B** (with $|J/a_N| << 1$) should relax similarly to the **PzNN** monoradical, hence it saturates much faster than the dominant component under a strong exchange limit ($|J/a_N| >> 1$). The comparison between the relaxation envelopes of **B** and **PzNN** at different microwave powers (see the Supporting Information) allows the subtraction from the observed Δm_s = 1 resonance envelope of **B** a weighted percentage of uncoupled biradical (ca. 20%), defined by the following spin Hamiltonian parameters: $g_{\|}$ = 2.0028, $g_{\perp}$ = 2.0086, $A_{\|}$ = 1.8 mT, $A_{\perp}$ = 0.22 mT, $A_{\|dip}$ = 1.05 mT, $A_{\perp dip}$ = 0.53 mT. The procedure provides the Δm_s = 1 EPR envelope of the strong exchange limit component (see B in Figure 8, lower trace) and gives an estimation of $|2D| \approx 6.2$ mT and $|D/hc|$ of around $2.9 \times 10^{-3}\ cm^{-1}$ for **B**. This is a much smaller zfs value than that found previously for **A** ($|D/hc| \approx 4.5 \times 10^{-3}\ cm^{-1}$).[13]

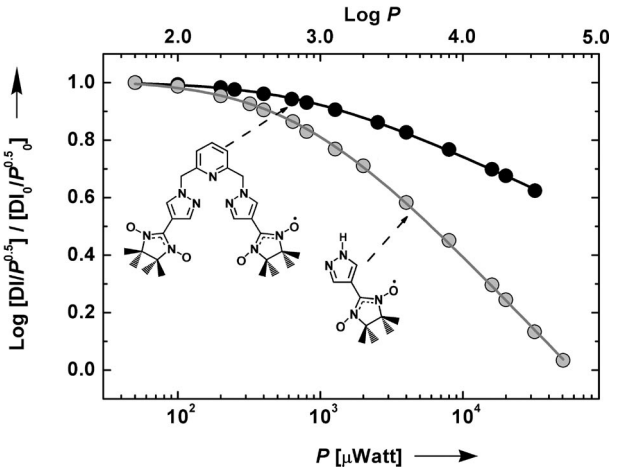

Figure 9. The EPR power saturation behaviour recorded at T = 122 K for the pyrazol-4-yl nitronyl nitroxide monoradical **PzNN** (●, experimental data) and the biradical **B** (●, experimental data). The solid lines correspond to the fitting results with parameters (b, $P½$) given in the text.

In the point-dipole approximation,[26] the estimated D value indicates an averaged distance between the centres of the ONĈNO groups of around 9.6 Å, a much smaller value than the averaged distance observed in the crystal (ca. 11.7 Å). In order to estimate the singlet–triplet energy separation (ΔE_{ST}) the EPR analyses were extended down to cryogenic temperatures. As shown in part D of Figure 8 the double integration of the half-field transition Δm_s = 2 signal (χ_{EPR}, ●) increases upon lowering the sample temperature, but the product $\chi_{EPR}T$ (●) versus T remains almost constant over the temperature range with indications of a small increase at the lowest temperatures. This finding indicates that net destabilization of the singlet–triplet equilibrium (ST) occurs below 4 K, thus only an estimate for the ST energy separation can be obtained from the trend, with $0.06\ cm^{-1} < \Delta E_{ST} = 2J/k_B < 0.6\ cm^{-1}$. Such strong attenuation of the exchange coupling mediated by C(sp^3) bonds is consistent with recent ΔE_{ST} findings for calix[4]arene nitronyl nitroxide[27] and nitroxide[28] biradical systems in which the through-bond exchange coupling pathway was topologically defined by the conformationally constrained radical–*m*-phenylene–C(sp^3)–*m*-phenylene–radical synthetic designs.

The bulk magnetic susceptibility (DC) measurements for polycrystalline samples of **B** are shown in Figure 10. At T = 298 K the observed value of 0.745 emu K mol^{-1} (2.44 μ_B with g = 2) is similar to the theoretically expected

0.750 emu K mol^{-1} (2.45 μ_B) for two isolated S = ½ spin systems and agrees with the high-temperature EPR spin-concentration results. Below 30 K, $\chi_m T$ starts to significantly decrease, reaching a value of 0.437 emu K mol^{-1} (1.87 μ_B) at 4.5 K. Because such a strong reduction of $\chi_m T$ is not witnessed in the low-temperature $\chi_{EPR} T$ measurements, in which **B** was magnetically diluted, the behaviour in the bulk confirms the dominating antiferromagnetic through-space interactions between radical centres, as observed previously in the X-ray structural analyses. These results indicate that the step-conformation adopted by **B** in the crystal lattice does not represent the main conformation of **B** in solution or in frozen solution. Data analysis was carried out by using the Curie–Weiss model, giving a Curie constant C = 0.750 emu mol^{-1} K^{-1} and an averaged through-space antiferromagnetic interaction θ = 1.99 cm^{-1} (R^2 = 0.987). Preliminary experiments were carried out by using **B** as an organic scaffold for metal coordination in order to probe the variation of the through-bond exchange interaction between spin carriers upon metal complexation, namely under conformational constraints. The diamagnetic metal ion Zn^{2+} was chosen for this purpose because it should restrain the conformational freedom without the addition of extra electrons. Incubation of **B** with $ZnCl_2$ in a 1:1 ratio in MeOH/ethyl acetate allowed the formation of the mononuclear **ZnB** complex. The EPR spectra of **ZnB** in solution and in frozen solution (parts A and D, respectively, in Figure 11) exhibit fingerprints for completely uncoupled radical moieties. A similar effect was observed in spin-labelled nitronyl nitroxide calix[4]arene cryptands upon coordination with the Zn^{2+} cation.[29] Incubation of **ZnB** with EDTA/MeOH allows the original envelopes to be restored, like those reported previously in Figure 8. This effect indicates that the zinc ion is relatively weakly bound to the N donors (pyridine and pyrazole), but remarkably enough, metal depletion occurs in solution without any degradation of the spin units.

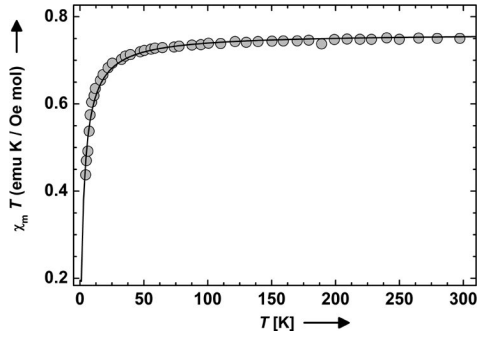

Figure 10. The bulk magnetic susceptibility χT vs. T for the biradical **B** recorded under an applied field B_0 of 1000 Oe. The symbol (●) represents experimental data and the solid line (——) the fitting analysis. Fitting parameters are discussed in main text.

Conclusions

A novel nitronyl nitroxide biradical system based on the 2,6-bis(pyrazolylmethyl)pyridine coupling core **B** has been described. The synthetic design allowed us to probe how the optical and magnetic properties of the system are influenced by the introduction of σ conjugation into the coupling unit core after comparison with the earlier reported π-conjugated 2,6-bis(pyrazolyl)pyridine nitronyl nitroxide biradical **A**. The presence of a non-alternant spin-polarization path through the organic backbone showed that the methylene carbon atoms (–CH_2–) carry positive spin densities (δ^+_C), as evidenced by paramagnetic ^{1}H NMR analysis in solution. In the presence of two C(sp^3) bonds, the triplet ground state (S = 1) is slightly preferred in **B**, with an estimated energy gap between this and the excited singlet (S = 0) of 0.06 cm^{-1} < ΔE_{ST} < 0.6 cm^{-1}; ΔE_{ST} in **B** is at least 20 times smaller than the singlet–triplet gap observed in **A** (ΔE_{ST} = 11.8 ± 4.8 cm^{-1}). Binding of the Zn^{2+} cation to the nitrogen donors of the bis(pyazolylmethyl)pyridine core induces decoupling of the radical units ($J \approx 0$), which now behave similarly to independent spins. Further work is currently underway to exploit the coordination properties of **B** as a spin probe for metal recognition and NO detection in biological membranes.

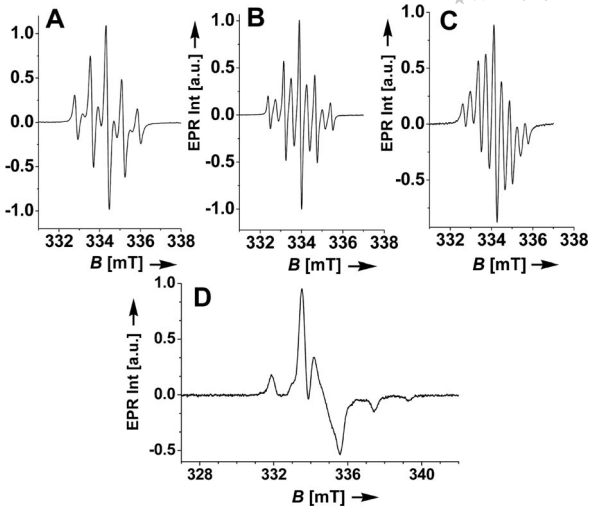

Figure 11. (A) X-band EPR spectra of **ZnB** (2×10^{-4} M, MeOH/toluene, 1:5, v/v) recorded in solution at T = 293 K with g_{iso} = 2.0065, a_N = 20.95 MHz. (B) As for (A) but recorded immediately after the addition of 5 equiv. of EDTA. (C) As for (A) but recorded after 30 min of incubation with. 5 equiv. of EDTA. (D) **ZnB** (2×10^{-4} M, MeOH/toluene, 1:5, v/v, g_{av} = 2.007) recorded in frozen solution at T = 122 K, showing the characteristic fingerprint of an isolated nitronyl nitroxide spin S = ½ system.

Experimental Section

General Remarks: All reagents (e.g., 2,6-bis(bromomethyl)pyridine, NaH, $NaIO_4$) and solvents from commercial sources were of the highest purity available and used as received. Tetrahydrofuran (THF) was dried by refluxing and distilling from metallic sodium in the presence of benzophenone. UV/Vis spectra were recorded with a Perkin–Elmer UV/Vis/NIR Lambda 900 spectrometer using a 1 cm optical-path quartz cell at room temperature. ^{1}H and ^{13}C NMR spectra were recorded with a Bruker AMX 250 or 300 Ultrashield spectrometer. IR spectra were measured in KBr pellets with a

Nicolet 730 FT-IR spectrometer at room temperature. Mass spectra were obtained with FD/FAB-MS VG Instruments ZAB-2 mass spectrometer. ICP analyses were performed with a Varian Vista AX CCD instrument. Elemental analyses were performed with a Foss Heraeus Varieo EL apparatus. Melting points were measured with a Büchi B-545 apparatus using open-ended capillaries and are uncorrected. ESR spectra were recorded in oxygen-free solutions (toluene) at a concentration of 10^{-4} mol dm^{-3} unless otherwise stated using a Bruker ESP300 E X-band spectrometer equipped with an NMR gaussmeter (Bruker ER035), a frequency counter (Bruker ER 041 XK) and a variable-temperature control continuous flow N_2 cryostat (Bruker B-VT 2000) or with the Oxford system (ESR 910) helium continuous flow cryostat. The *g* factor corrections were obtained by using the PNT radical [g = 2.0026(1)] or DPPH [g = 2.0037(1)] as references. Simulation of the room-temperature EPR spectrum was carried out by using the BiRad program as described previously.[13,15] The temperature-dependent static susceptibility (DC) of a powdered sample of **B** (28 mg) was recorded by using a Faraday-type magnetometer in the temperature range 4.5–298 K. The measurements were made by using a computer-controlled Cahn D-200 microbalance and a Bruker B-MN 200/60 power supply. Diamagnetic correction of the molar magnetic susceptibility (-3.68×10^{-4} cm^3 mol^{-1}) was obtained by using Pascal's constants. 4-Formyl-1*H*-pyrazole[13,15] (**1**) and 2,3-dimethyl-2,3-bis(hydroxyamino)butane[8] (**4**) were synthesized according to published procedures.

EPR Microwave Power Saturation Experiments: The magnitude of the observed EPR signal for paramagnetic species is proportional to the net resultant polarization of the spin orientations. However, the system is said to be saturated when the rates of upward and downward transitions are equal. This implies that no net energy is transferred between the external applied field and the spin system. Such an effect can be induced by working at high microwave power. The empirical expression used to fit the saturation EPR data follows the work of Portis and Castner[23] and it is expressed by Equation (2) where *DI* is the double-integrated signal intensity, *P* is the applied microwave power, *b* is the relaxation factor (b = 1 for inhomogeneous line-broadening and b = 3 for homogeneous line-broadening) for a first derivative spectrum as it is usually acquired within common EPR experiment, $P½$ is the power at which half the signal is saturated and *k* is an experimental constant associated with the instrument. The value of *b* depends on which mechanism is dominating within the relaxation process of the quanta being adsorbed, that is, if the spin-lattice relaxation (T_1) represents the dominant factor, the power-dependent line-broadening is inhomogeneous (Gaussian line) and *b* assumes the minimum value, namely b = 1. When T_2 is dominant, the line-broadening is homogeneous (Lorentzian line) and *b* assumes the maximum value of 3. The relaxation factor is often allowed to fluctuate in the fitting in order to account for intermediate cases ($1 \leq b \leq 3$), when the line shape observed is a mixture of Lorentzian and Gaussian lines.

$$DI = k\sqrt{P}/[(1+P/P_{½})]^{b/2} \quad (2)$$

In order to apply Equation (2) the following experimental conditions must be satisfied: 1) the samples should be in a region of the cavity with maximum microwave field (H_1) so the filling factor has to be optimized, 2) the sample temperature must be constant and 3) the Zeeman modulation amplitude, the frequency and possibly the gain must also be constant. Equation (2), however, is not strictly applicable when dipolar couplings and/or exchange interactions are present in the system because the half-saturation power ($P½$) is defined by Equation (3) and Equation (4) where *V* represents the cavity volume, *Q* the cavity quality factor ($Q = H_1^2 V/2P$), *P* the power dissipated in the cavity and γ the giromagnetic ratio. Equation (3) assumes that all spins at resonance saturate equivalently and hence they show the same product for (T_1T_2). When dipolar and/or exchange interactions are present, the product (T_1T_2) is no longer constant and *b* is found to be smaller than 1.[24,25]

$$P_{½} = [a/(T_1T_2)] \quad (3)$$

$$a = ½(V/Q\gamma^2) \quad (4)$$

2,6-Bis(4-formylpyrazolylmethyl)pyridine (3): NaH was added (0.24 g, 10 mmol) to a solution of 4-formyl-1*H*-pyrazole (1 g, 10.4 mmol) in dry THF (30 mL) and then the mixture was heated under argon at 50 °C while stirring for 20 min. After addition of 2,6-bis(bromomethyl)pyridine (1.32 g, 5 mmol), the temperature was raised to 60 °C and the reaction left at this temperature for 3 h. The solution containing the product was cooled down to room temperature and the solvent was removed under reduced pressure leaving a pale yellowish residue that was collected and poured into a water/ice mixture. A white solid was collected after filtration. Recrystallization of the solid from ethanol/water mixture (1:1, v/v) afforded analytically pure 2,6-bis[(4-formylpyrazolyl)methyl]pyridine (**3**, 0.8 g, yield 54%). M.p. 106–107 °C (from water). FTIR (KBr): $\tilde{\nu}$ = 3108 (m), 3061 (w), 2969 (w), 2845 (w), 2789 (w), 1683 ($\nu_{C=O}$, s), 1595 (m), 1573 (m), 1544 (s), 1456 (m), 1420 (m), 1324 (m), 1197 (s), 1162 (s), 1091 (m), 997 (s), 985 (w), 967 (w), 894 (m), 872 (m), 761 (s), 631 (s) cm^{-1}. ^{1}H NMR ($CDCl_3$, 250 MHz, 298 K): δ = 5.4 (s, 4 H, 2-CH_2), 7.11–7.14 (d, $^3J_{H,H}$ = 8.0 Hz, 2 H, 2-CH), 7.66–7.73 (t, $^3J_{H,H}$ = 8.0 Hz, 1 H, CH), 7.96 (s, 2 H, 2-CH), 8.05 (s, 2 H, 2-CH), 9.83 (s, 2 H, 2-CHO) ppm. ^{13}C NMR ($CDCl_3$, 63 MHz, 298 K): δ = 57.6, 121.6, 124.7, 133.6, 138.4, 141.0, 154.8, 183.9 ppm. FDMS (70 eV, $CHCl_3$): *m*/*z* (%) = 295.1 (100). $C_{15}H_{13}N_5O_2 \cdot H_2O$ (295.30): calcd. C 57.50, H 4.83, N 22.35; found C 57.30, H 4.94, N 22.24.

2,6-Bis[4-(1,3-dihydroxy-4,4,5,5-tetramethylimidazolidin-2-yl)-pyrazolylmethyl]pyridine (5): 2,6-Bis[(4-formylpyrazolyl)methyl]pyridine (**3**, 590 mg, 2 mmol) and 2,3-bis(hydroxyamino)-2,3-dimethylbutane (**4**, 600 mg, 4 mmol) were charged into a small flask with methanol (40 mL) and stirred under argon for 48 h. The white solid product was filtered off, washed with water and cold ethanol (–10 °C) and then air-dried to give 2,6-bis[4-(1,3-dihydroxy-4,4,5,5-tetramethylimidazolidin-2-yl)pyrazolylmethyl]pyridine which was used for the next oxidation step without further purification (690 mg, yield 62%). M.p. 148–149 °C (from water, it decomposes before melting changing colour from white to deep-red). FTIR (KBr): $\tilde{\nu}$ = 3238 (br, ν_{OH}) 2976 (s), 2929 (s), 1599 (m), 1575 (s), 1459 (s), 1421 (s), 1363 (s), 1311 (w), 1209 (w), 1174 (s), 1145 (s), 1093 (w), 1022 (m), 999 (s), 964 (w), 935 (w), 912 (m), 843 (m), 802 (m), 762 (s), 695 (w), 665 (w) cm^{-1}. ^{1}H NMR ([D_6]DMSO, 250 MHz, 298 K): δ = 1.00–1.05 (dd, 24 H, 8-CH_3), 4.56 (s, 2 H, 2-CH), 5.38 (s, 4 H, 2-CH_2), 6.90 (d, $^3J_{H,H}$ = 8.0 Hz, 2 H, 2-CH), 7.45 (s, 2 H, 2-CH), 7.77 (m, 5 H, 1-CH + 4-OH), 8.32 (s, 2 H, -CH) ppm. ^{13}C NMR ([D_6]DMSO, 63 MHz, 298 K): δ = 16.8, 23.4, 56.0, 65.4, 78.7, 82.9, 119.9, 122.6, 129.6, 138.6, 156.3 ppm. $C_{27}H_{41}N_9O_4$ (555.67): calcd. C 58.36, H 7.44, N 22.69; found C 58.04, H 7.66, N 22.36.

2,6-Bis[4-(1-oxyl-3-oxido-4,4,5,5-tetramethylimidazolin-2-yl)-pyrazolylmethyl]pyridine (B): 2,6-Bis[4-(1,3-dihydroxy-4,4,5,5-tetramethylimidazolidin-2-yl)pyrazolylmethyl]pyridine (**5**, 555 mg, 1 mmol) was oxidized by $NaIO_4$ (540 mg, 2.5 mmol) under phase-transfer conditions in water/chloroform (1:1, v/v) for 60 min. The

organic phase became deep-blue after 20 min. After collection and evaporation of the organic phase, the product was purified by flash chromatography over SiO_2 using acetone/petroleum ether (low boiling point, 4:6) as eluent (R_f = 0.28) to afford the radical product **B** as a blue solid (355 mg, yield 64%). M.p. 169–170 °C (from acetone). FTIR (KBr): $\tilde{\nu}$ = 3145 (w), 2977 (s), 2987 (m), 2931 (m), 1672 (w), 1598 (m), 1573 (w), 1541 (w), 1460 (s), 1427 (m), 1403 (m), 1365 (s, ν_{N-O}), 1317 (m), 1219 (w), 1196 (m), 1174 (m), 1138 (m), 1016 (m), 993 (d), 868 (m), 813 (w), 773 (m) 659 (m) cm^{-1}. UV/Vis (toluene) λ (ε) 651 (2420), 597 (2216), 550 (1023), 352 (44060), 336 (18660 $M^{-1} cm^{-1}$) nm. FABMS (NB matrix): *m/z* (%) = 550.3 (100) $[M + H]^+$. $C_{27}H_{35}N_9O_4$ (549.63): calcd. C 59.00, H 6.42, N 22.94; found C 58.73, H 6.50, N 22.78.

Synthesis of {2,6-Bis[4-(1-oxyl-3-oxido-4,4,5,5-tetramethylimidazolin-2-yl)pyrazolylmethyl]pyridine}zinc Dichloride (ZnB): In a round-bottomed flask, the diradical **B** (84 mg, 0.153 mmol) was dissolved in MeOH/ethyl acetate (10 mL, 1:1, v/v) and left at room temperature whilst stirring. Then $ZnCl_2$ powder (21 mg, 0.153 mmol) was added and the reaction mixture was warmed at 55 °C for 30 min. Upon cooling, part of the solvent was evaporated to about half of the initial volume and diethyl ether was added (10 mL). A bluish precipitate of **ZnB** formed quickly which was collected by filtration and dried under vacuum (90 mg, yield 86%). $C_{27}H_{35}N_9O_4ZnCl_2 \cdot 2H_2O$ (721.96): calcd. C 44.90, H 5.40, N 17.46; found C 44.63, H 5.53, N 17.38. ICP: calcd. for $C_{27}H_{35}N_9O_4ZnCl_2 \cdot H_2O$: Zn 9.06%; found Zn 8.88%. UV/Vis (MeOH/toluene, 1:5): λ (ε) = 648 (2170), 596 (2100), 549 (1100), 350 (36260), 334 (18000 $M^{-1} cm^{-1}$) nm.

Crystal Structure Determination of 2,6-Bis[4-(1-oxyl-3-oxido-4,4,5,5-tetramethylimidazolin-2-yl)pyrazolylmethyl]pyridine (B): Crystals of **B** were grown in $CHCl_3$ solution under slow vapour diffusion of hexane in the dark and at room temperature over three days, forming blue prisms of crystalline material. The structure was then solved by direct methods and refined by a full-matrix least-squares procedure.[30] The crystallographic data were collected on Nonius-Kappa CCD (MoK_α, μ = 0.71073 Å) diffractometer equipped with a graphite monochromator.

CCDC-664335 contains the supplementary crystallographic data for this paper. These data can be obtained free of charge from The Cambridge Crystallographic Data Centre via www.ccdc.cam.ac.uk/data_request/cif.

Supporting Information (see footnote on the first page of this article): ^1H and ^{13}C NMR spectra of compounds **5** and **B**, EPR spectra of **PzNN** in solution, EPR-power-saturation behaviours of **PzNN** and biradical **B** in frozen solution, fluorescence spectra of biradicals **A** and **B**.

Acknowledgments

G. Z., A. G., V. E. and M. B. thank the Max Planck Society for continuing support. G. Z. and K. K. A. thank the Research Council of Norway for a grant (177661/V30, to K. K. A.). Prof. Dr. W. Haase and Dr. K. Falk (TU Darmstadt) are acknowledged for the susceptibility measurements performed on **B**.

[1] a) J. H. Osiecki, E. F. Ullman, *J. Am. Chem. Soc.* **1968**, *90*, 1078–1079.
[2] E. F. Ullman, L. Call, J. H. Osiecki, *J. Org. Chem.* **1970**, *35*, 3623–3631.
[3] E. F. Ullman, J. H. Osiecki, D. G. B. Boocock, R. Darcy, *J. Am. Chem. Soc.* **1972**, *94*, 7049–7059.
[4] a) O. Kahn, *Magnetism: A Supramolecular Function*, Kluwer, Dordrecht, **1996**; b) J. S. Miller, M. Drillon, *Magnetism: Molecules to Materials*, Wiley-VCH, Weinheim, **2003**, vol. I, II, IV.
[5] a) M. Tamura, Y. Nakazawa, D. Shiomi, K. Nozawa, Y. Hosokoshi, M. Ishikawa, M. Takahashi, M. Kinoshita, *Chem. Phys. Lett.* **1991**, *186*, 401–404; b) M. Kinoshita, P. Turek, M. Tamura, K. Nozawa, D. Shiomi, Y. Nakazawa, M. Ishikawa, M. Takahashi, K. Awaga, T. Inabe, Y. Maruyama, *Chem. Lett.* **1991**, 1225–1229; c) J. Cirujeda, E. Hernàndez-Gasió, C. Rovira, J.-L. Stanger, P. Turek, J. Veciana, *J. Mater. Chem.* **1995**, *5*, 243–252; d) J. Cirujeda, M. Mas, E. Molins, F. L. Panthou, J. Laugier, J. G. Park, C. Paulsen, P. Rey, C. Rovira, J. Veciana, *J. Chem. Soc. Chem. Commun.* **1995**, 709–710; e) M. M. Matsushita, A. Izuoka, T. Sugawara, T. Kobayashi, N. Wada, N. Takeda, M. Ishikawa, *J. Am. Chem. Soc.* **1997**, *119*, 4369–4379; f) C. Hirel, D. Luneau, J. Pécaut, L. Öhrström, G. Bussière, C. Reber, *Chem. Eur. J.* **2002**, *8*, 3157–3161.
[6] a) D. A. Shultz, S. H. Bodnar, K. E. Vostrikova, J. W. Kampf, *Inorg. Chem.* **2000**, *39*, 6091–6093; b) H. O. Stumpf, L. Ouahab, Y. Pei, D. Grandjean, O. Kahn, *Science* **1993**, *261*, 447–449; c) K. Inoue, T. Hayamizu, H. Iwamura, D. Hashizume, Y. Ohashi, *J. Am. Chem. Soc.* **1996**, *118*, 1803–1804; d) G. Ballester, E. Coronado, C. Giménez-Saiz, F. Romero, *Angew. Chem. Int. Ed.* **2001**, *40*, 792–795; e) K. Fegy, D. Luneau, T. Ohm, C. Paulsen, P. Rey, *Angew. Chem. Int. Ed.* **1998**, *37*, 1270–1273; f) C. Benelli, D. Gatteschi, *Chem. Rev.* **2002**, *102*, 2369–2387; g) K. Inoue, H. Iwamura, *J. Am. Chem. Soc.* **1994**, *116*, 3173–3174; h) F. Mathevet, D. Luneau, *J. Am. Chem. Soc.* **2001**, *123*, 7465–7466; i) C. Rajadurai, V. Enkelmann, V. Ikorskii, V. Ovcharenko, M. Baumgarten, *Inorg. Chem.* **2006**, *45*, 9664–9669; j) K. Bernot, L. Bogani, A. Caneschi, D. Gatteschi, R. Sessoli, *J. Am. Chem. Soc.* **2006**, *128*, 7947–7956.
[7] a) J. Joseph, B. Kalyanaraman, J. S. Hyde, *Biochem. Biophys. Res. Commun.* **1993**, *192*, 926–934; b) T. Nagano, T. Yoshimura, *Chem. Rev.* **2002**, *102*, 1235–1270; c) P. Cabrales, A. G. Tsai, M. Intaglietta, *J. Appl. Physiol.* **2005**, *100*, 1181–1187.
[8] a) C. Hirel, E. K. Vostrikova, J. Pécaut, V. I. Ovcharenko, P. Rey, *Chem. Eur. J.* **2001**, *7*, 2007–2014; b) P. Wautelet, J. Le Moigne, V. Videva, P. Turek, *J. Org. Chem.* **2003**, *68*, 8025–8036.
[9] a) J. S. Miller, A. Epstein, *Angew. Chem. Int. Ed. Engl.* **1994**, *33*, 385–415; b) S. Nakatsuji, H. Anzai, *J. Mater. Chem.* **1997**, *7*, 2161–2174.
[10] a) J. A. Crayston, J. N. Devine, J. C. Walton, *Tetrahedron* **2000**, *56*, 7829–7857; b) A. Rajca, *Chem. Rev.* **1994**, *94*, 871–893.
[11] a) H. C. Longuet-Higgins, *J. Chem. Phys.* **1950**, *18*, 265–274; b) W. T. Borden, E. R. Davidson, *J. Am. Chem. Soc.* **1977**, *99*, 4587–4594; c) A. A. Ovchinnikov, *Theor. Chim. Acta* **1978**, *47*, 297–304; d) P. M. Lahti, *Magnetic Properties of Organic Materials*, Marcel Dekker, New York, **1999**.
[12] a) D. A. Dougherty, *Acc. Chem. Res.* **1991**, *24*, 88–94; b) W. T. Borden, *Mol. Cryst. Liq. Cryst.* **1993**, *232*, 195–218; c) W. T. Borden, H. Iwamura, J. A. Berson, *Acc. Chem. Res.* **1994**, *27*, 109–116; d) P. Lafuente, J. J. Novoa, M. J. Beapark, P. Celani, M. Olivucci, M. A. Robb, *Theor. Chim. Acta* **1999**, *102*, 309–316; e) K. Hayakawa, D. Shiomi, T. Ise, K. Stao, T. Takui, *J. Mater. Chem.* **2006**, *16*, 4146–4154.
[13] G. Zoppellaro, A. Geies, V. Enkelmann, M. Baumgarten, *Eur. J. Org. Chem.* **2004**, 2367–2374.
[14] M. A. Halcrow, *Coord. Chem. Rev.* **2005**, *249*, 2880–2908.
[15] G. Zoppellaro, V. Enkelmann, A. Geies, M. Baumgarten, *Org. Lett.* **2004**, *6*, 4929–4932.
[16] L. Catala, R. Feher, D. B. Amabilino, K. Wurst, J. Veciana, *Polyhedron* **2001**, *20*, 1563–1569.
[17] G. Zoppellaro, A. Ivanova, V. Enkelmann, A. Geies, M. Baumgarten, *Polyhedron* **2003**, *22*, 2099–2110.
[18] a) M. M. Matsushita, A. Izuoka, T. Sugawara, T. Kobayashi, N. Wada, N. Takeda, M. Ishikawa, *J. Am. Chem. Soc.* **1997**, *119*, 4369–4379; b) L. Zhang, Z. L. Liu, L. H. Weng, D. Z. Liao, Z. H. Jiang, S. P. Yan, P. W. Shen, M. Baumgarten, *Helv.*

Chim. Acta **2001**, *84*, 834–841; c) C. Rajadurai, A. Ivanova, V. Enkelmann, M. Baumgarten, *J. Org. Chem.* **2003**, *68*, 9907–9915; d) C. Stroh, M. Mayor, C. von Hänisch, *Tetrahedron Lett.* **2004**, *45*, 9623–9626; e) C. Stroh, R. Ziessel, G. Raudaschl-Sieber, F. H. Köhler, P. Turek, *J. Mater. Chem.* **2005**, *15*, 850–858.

[19] a) R. E. Kreilick, J. Becker, E. F. Ullman, *J. Am. Chem. Soc.* **1969**, *91*, 5121–5124; b) M. S. Davis, K. Morokuma, R. E. Kreilick, *J. Am. Chem. Soc.* **1972**, *94*, 5588–5592; c) J. P. Jesson, *J. Chem. Phys.* **1967**, *47*, 579; d) J. Goldman, T. E. Peterson, K. Torssell, J. Becker, *Tetrahedron* **1973**, *29*, 3833–3843.

[20] E. Tretyakov, S. Fokin, G. Romanenko, V. Ikorskii, S. Vasilevsky, V. Ovcharenko, *Inorg. Chem.* **2006**, *45*, 3671–3678.

[21] A. Bencini, D. Gatteschi, *Electron Paramagnetic Resonance of Exchange Coupled Systems*, Springer, Berlin, **1990**, chapter 3.

[22] a) P. W. Anderson, *Phys. Rev.* **1959**, *115*, 2–13; b) O. Kahn, *Molecular Magnetism*, Wiley-VCH, New York, **1993**, chapter 8; c) P. J. Hai, J. C. Thibeault, R. Hoffman, *J. Am. Chem. Soc.* **1975**, *97*, 4884–4899; d) C. Kaneda, D. Shiomi, K. Sato, T. Takui, *Polyhedron* **2003**, *22*, 1809–1816; e) K. Maekawa, D. Shiomi, T. Ise, K. Sato, T. Takui, *J. Phys. Chem. B* **2005**, *109*, 3303–3309.

[23] a) A. M. Portis, *Phys. Rev.* **1953**, *91*, 1071–1078; b) T. J. Castner Jr, *Phys. Rev.* **1959**, *115*, 1506–1515.

[24] D. J. Hirsh, G. W. Brudvig, *Nat. Protocols* **2007**, *2*, 1770–1781.

[25] a) C. Galli, J. B. Innes, D. J. Hirsh, G. W. Brudvig, *J. Magn. Reson.* **1996**, *110*, 284–287; b) C. Galli, M. Atta, K. K. Andersson, A. Gräslund, G. W. Brudvig, *J. Am. Chem. Soc.* **1995**, *117*, 740–746; c) H. Sigel, *Metal Ions in Bilogical Systems*, Marcel Dekker, New York, **1987**, vol. 22, chapter 4.

[26] a) K. Mukai, T. Tamaki, *Bull. Chem. Soc. Jpn.* **1977**, *50*, 1239–1244; b) J. A. Weil, J. R. Bolton, J. E. Wertz, *Electron Paramagnetic Resonance*, VCH, Weinheim, **1994**, p. 174; c) K. A. Sandberg, D. A. Shultz, *J. Phys. Org. Chem.* **1998**, *11*, 819–824.

[27] A. Rajca, M. Pink, S. Mukherjee, S. Rajca, K. Das, *Tetrahedron* **2007**, *44*, 10731–10742.

[28] A. Rajca, S. Mukherjee, M. Pink, S. Rajca, *J. Am. Chem. Soc.* **2006**, *41*, 13497–13507.

[29] G. Ulrich, P. Turek, R. Ziessel, *Tetrahedron Lett.* **1996**, *37*, 8755–8758.

[30] a) G. M. Sheldrick, *SHELXS-86, Program for Crystal Structure Solution*, Institut für Anorganische Chemie der Universität Göttingen, Germany, **1986**; b) P. W. Betteridge, J. R. Carruthers, R. I. Cooper, K. Prout, D. J. Watkin, *J. Appl. Crystallogr.* **2003**, *36*, 1487.

Received: November 7, 2007
Published Online: January 29, 2008

